Optical and Microphysical Properties of Upper Clouds Measured with the Raman Lidar and Hydrometeor Videosonde: A Case Study on 29 March 2004 over Tsukuba, Japan

TETSU SAKAI*

A 21st Century COE Program, Graduate School of Environmental Studies, Nagoya University, Nagoya, Japan

NARIHIRO ORIKASA, TOMOHIRO NAGAI, MASATAKA MURAKAMI, KENICHI KUSUNOKI, AND KAZUMASA MORI+

Meteorological Research Institute, Tsukuba, Japan

AKIHIRO HASHIMOTO

Advanced Earth Science and Technology Organization, Meteorological Research Institute, Tsukuba, Japan

TAKATSUGU MATSUMURA

Japan Science and Technology Agency, Meteorological Research Institute, Tsukuba, Japan

TAKASHI SHIBATA

Graduate School of Environmental Studies, Nagoya University, Nagoya, Japan

(Manuscript received 6 June 2005, in final form 28 November 2005)

ABSTRACT

Optical and microphysical properties of the upper clouds at an altitude range of 5–11 km were measured over Tsukuba, Japan, on 29–30 March 2004 using a ground-based Raman lidar and a balloon-borne hydrometeor videosonde (HYVIS). The Raman lidar measured the vertical distributions of the particle extinction coefficient, backscattering coefficients, depolarization ratio, and extinction-to-backscatter ratio (lidar ratio) at 532 nm; further, it measured the water vapor mixing ratio. The HYVIS measured the vertical distributions of the particle size, shape, cross-sectional area, and number concentration of the cloud particles by taking microscopic images. The HYVIS measurement showed that the cloud particles were ice crystals whose shapes were columnar, bulletlike, platelike, and irregular, and 7–400 μm in size. The Raman lidar measurement showed that the depolarization ratio ranged from 0% to 35% and the lidar ranged from 0.3 to 30 sr for the clouds in ice-saturated air. The comparison between the measured data and theoretical calculations of the cloud optical properties suggests that the observed variations in the depolarization ratio and lidar ratio were primarily due to the variation in the proportion of the horizontally oriented ice crystals in the clouds. The optical thickness of the cloud obtained from the lidar was about 2 times lower than that calculated from the HYVIS data, and the maximum extinction coefficient was about 5 times lower than the HYVIS data. The most probable reason for the differences is the horizontal inhomogeneities of the cloud properties between the measurements sites for the two instruments.

1. Introduction

Cirrus clouds frequently appear in the upper troposphere and can affect the earth's climate. They can affect the radiation balance by scattering and absorbing the solar and terrestrial radiation and can affect the hydrological cycles through precipitation processes (Liou 1986; Stephens 2002). To understand the effects of these clouds on climate, it is necessary to measure the temporal and spatial distributions of their microphysical properties such as phase, shape, size, number concentration, orientation, and the optical properties. Lidar is a useful tool for measuring the vertical distribution of the optical properties of cirrus clouds. However, the applications of the lidar measurement to the cirrus cloud studies are rather limited partly due to the lack of knowledge pertaining to the rela-

* Current affiliation: Meteorological Research Institute, Tsukuba, Japan.

+ Current affiliation: Atmospheric Environment Division, Japan Meteorological Agency, Tokyo, Japan.

Corresponding author address: Tetsu Sakai, Nagamine 1-1, Tsukuba, Ibaraki 305-0052, Japan.
E-mail: tetsu@mri-jma.go.jp

© 2006 American Meteorological Society

tion between the derived optical properties and the microphysical properties. Several measurement studies compared the lidar-derived optical properties with the in situ cloud microphysical properties. Sassen et al. (2003) compared the lidar-derived depolarization ratio with the ice crystal images taken by the aircraft-mounted replicator for the cirrus clouds derived from a hurricane or tropical flow in the midlatitude. Whiteway et al. (2004) compared the vertical structure of the lidar-derived backscattering ratio with that of the images of the particles for the cirrus produced by frontal systems and tropical convection. Hogan et al. (2003) compared the lidar-derived extinction coefficients with those calculated from the airborne hot-wire probe data for the mixed-phase clouds over England. Although these studies have revealed the relation between the optical and microphysical properties of the clouds, most of the studies have employed the elastic and polarization lidar technique and compared these properties qualitatively or semiquantitatively. The Raman lidar technique is also useful for cirrus cloud studies since it measures the extinction coefficient by detecting the inelastic Raman backscattering of nitrogen molecules (Ansmann et al. 1992a; Ansmann 2002; Whiteman 2003) as well as the backscattering coefficient by detecting the elastic backscattering of cloud particles and molecules. From these coefficients we can obtain an additional intensive optical property: extinction-to-backscatter ratio or lidar ratio. Reichardt et al. (2002) have studied the relation between the lidar and depolarization ratios of cirrus clouds over the Arctic, and determined their negative and positive correlations that are dependent on temperature.

To study the relation between these optical properties obtainable using the Raman lidar and the in-situ microphysical properties of the clouds, a measurement of the upper clouds using the Raman lidar and balloon-borne hydrometeor videosonde (HYVIS) was carried out over Tsukuba, Japan, on 29–30 March 2004. The HYVIS is a compact and lightweight instrument that measures the vertical distribution of the microphysical properties of clouds (particle shape, size, cross-sectional area, and number concentration) by taking microscopic images onboard a balloon. Using this instrument, Mizuno et al. (1994) observed the microstructures of cirrostratus clouds, Murakami et al. (1992) observed warm frontal clouds, and Kusunoki et al. (2004) observed orographic snow clouds. Because it can measure clouds with high vertical resolution (~60 m) and its measurement setup is less expensive and simpler than that on an aircraft, it might be useful for the validation of the lidar measurements of cirrus optical properties.

TABLE 1. Specifications of the Raman lidar at MRI.

Transmitter			
Laser type	Nd:YAG		
Wavelength	532 nm		
Energy/pulse	~700 mJ		
Repetition rate	30 Hz		
Beam divergence	0.125 mrad (after collimator)		
Receiver			
Telescope type	Cassegrain		Cassegrain
Diameter	1.0 m (Raman and elastic)		0.35 m (elastic polarization)
Field of view	2.0 mrad		1.5 mrad
Detector	PMT (Hamamatsu R1333, R1332)		
Signal detection	Photon counting		
Range resolution	6 m (maximum)		
Temporal resolution	3 min		
Detection species	Raman H_2O	Raman N_2	Elastic polarization
Interference filter			
Center wavelength (nm)	660.5	607.3	532.0
Full width at half maximum (nm)	0.55	0.49	0.49

This paper reports the preliminary results of a comparison between cloud properties measured for the first time using the Raman lidar and HYVIS. Section 2 describes the instruments used in this study. Section 3 shows the results of the measurement of the cloud properties obtained using the lidar and HYVIS. The depolarization ratio and lidar ratio obtained using the lidar were compared with those calculated theoretically for the cloud particles in order to understand the observed variations in these values. Further, a comparison between the cloud extinction coefficient profiles obtained using the lidar and those calculated from HYVIS data was also conducted. A summary of this study is given in section 4.

2. Instrumentations

a. Raman lidar

The Raman lidar measures the vertical distributions of the optical properties of the clouds and aerosols as well as the water vapor mixing ratio (Whiteman 2003; Ansmann et al. 1992b). We used the Raman lidar developed by the Meteorological Research Institute (MRI), Japan. Table 1 shows the main characteristics of the lidar. The details of the lidar system and data analysis procedure are described by Sakai et al. (2003). The lidar transmits laser pulses at a wavelength of 532 nm vertically into the atmosphere and collects the inelastically backscattered (Raman backscattered) light by the

nitrogen molecules at 607 nm and the water vapor at 660 nm and the elastically backscattered (Mie and Rayleigh backscattered) light by the cloud/aerosol particles and molecules at 532 nm using Cassegrainian telescopes. The derived parameters are the backscattering ratio (R), particle backscattering coefficient (β), extinction coefficient (α), depolarization ratio (δ), lidar ratio (S), and the water vapor mixing ratio (w). The value of δ is defined by the ratio of the perpendicularly polarized component to the total component of the particle backscattering coefficient with respect to the polarization plane of the emitted laser light. This value can be considered as a measure of the nonsphericity of the particles; the value is zero for homogeneous spherical particles and substantially deviates from zero for the randomly oriented nonspherical particles whose size is larger than the laser wavelength (Mishchenko and Sassen 1998). The value of S is defined by the ratio of the particle extinction coefficient to backscattering coefficient. This value depends on the particle size, shape, and chemical composition. For example, based on field observations (Ferrare et al. 2001; Anderson et al. 2000) and theoretical calculations (Ackermann 1998), the values for submicrometer-sized aerosols are generally higher than approximately 30 sr. Meanwhile, the values for the supermicrometer-sized ice crystals and water droplets are generally lower than 30 sr (Sakai et al. 2003). Since the lidar was vertically pointing in this study, the δ and S values also depend on the particle orientation for the large ice crystals. For example, horizontally oriented ice crystals show near zero-δ values and low S values (<1 sr) due to specular reflections (Liou and Lahore 1974; Platt et al. 1978; Mishchenko et al. 1997; Yang et al. 2003). It should be noted that the multiple scattering can affect the α (and S) values (underestimate by as much as up to 50%) for the cloud particles by reducing the apparent extinction (Wandinger 1998; Reichardt et al. 2000; Sakai et al. 2003). This effect is further discussed in section 3d. The relative humidity was calculated from the lidar-derived w and the radiosonde-derived temperature and pressure.

The vertical resolution of the analyzed data was 197 m and the temporal resolution was 9 min except in the case of the high-resolution data of R and δ, shown in Figs. 1a,b with resolutions 96 m and 3 min. The uncertainty in the analyzed data was calculated using Poisson statistics for the observed photon counts.

b. Hydrometeor videosonde

The hydrometeor videosonde measures the vertical distributions of the microphysical properties of cloud particles by taking microscopic images on board the balloon. Details of the HYVIS are described by Murakami and Matsuo (1990) and Orikasa and Murakami (1997). The dimensions of the HYVIS instrument are 280 mm $\times$ 106 mm $\times$ 500 mm, and its weight is approximately 2.4 kg. All the instruments are on board a 1.5-kg balloon. The HYVIS collects cloud particles through an inlet that is 1 cm in diameter with a suction fan and samples them on the surface of a transparent 35-mm leader film coated with silicon oil. The particle collection efficiency is estimated to be 100% for the cloud particles larger than 10 μm at 200 hPa (Orikasa and Murakami 1997). Microscopic images of the particles are taken using two small video cameras with different magnifications. The detectable particle size range is 7 μm–5 mm in the maximum dimension. Nighttime measurement is performed by illuminating the particles with an electric light. The images are transmitted in real time to a ground receiver by 1687-MHz microwaves. The microphysical properties obtainable from the cloud microscopic images are the particle shape, size, cross-sectional area, and the number concentration. These properties were analyzed manually. The temporal resolution of the data is approximately 10 s, which corresponds to the vertical resolution of approximately 67 m (ascending speed of the balloon with an average of 6.7 m s^{-1} in this study). In this study, the average number of cloud particles collected in 10 s was 135. For comparison with the lidar data, the HYVIS-derived data were averaged vertically for 250 m. In this vertical range, the HYVIS obtained three or four particle images at two magnifications.

In addition to the HYVIS, the radiosonde (RS-01G, Meisei Electronic Co., Ltd.) measured the atmospheric pressure, temperature, and relative humidity. Further, a chilled mirror hygrometer (SnowWhite, meteolabor AG), on board the same balloon, measured the dew/frost points.

3. Results

The measurement of the upper clouds was made during the nighttime period of 29–30 March 2004 over Tsukuba (36.1°N, 140.1°E, 27 m above mean sea level), located in the central part of the Kanto Plain in Japan. During the measurement period, a high pressure had been covering the measurement site. The Raman lidar measured the atmospheric vertical profiles for the period ranging from 1738 local standard time (LST) 29 March to 0628 LST 30 March. The balloon equipped with the HYVIS instruments was launched at 1837 LST on 29 March about 250 m northeast of the lidar site. The balloon reached a height of 12 km and drifted about 40 km east from the launching site 30 min after

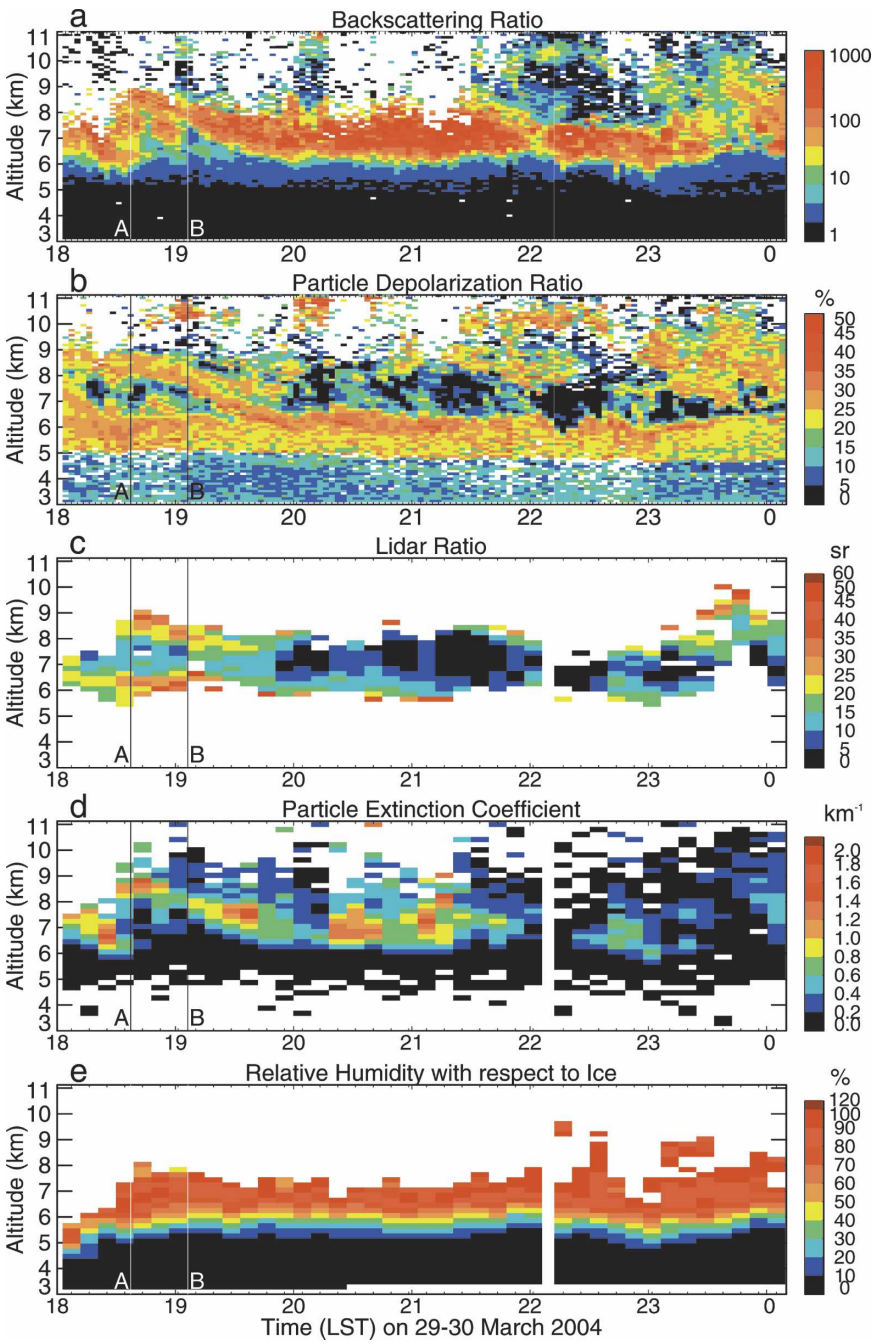

FIG. 1. Temporal and vertical cross section of (a) the backscattering ratio, (b) particle depolarization ratio, (c) lidar ratio, (d) extinction coefficient, and (e) relative humidity with respect to ice obtained using the Raman lidar for 29–30 Mar 2004 over Tsukuba. The vertical lines denote the times when the HYVIS-mounted balloon was launched (A) and reached an altitude of 12 km (B). The data with large uncertainties due to the weak signal intensity were not shown.

the launch. During the period of the HYVIS measurement, thin cirrus clouds, which blurred the outline of the Moon, were visible. The HYVIS obtained 87 images of the cloud particles at each magnification.

a. Raman lidar data

Figure 1 shows the vertical and temporal cross section of R, δ, S, α, and the relative humidity with respect to ice (RHi) obtained by the Raman lidar for the period

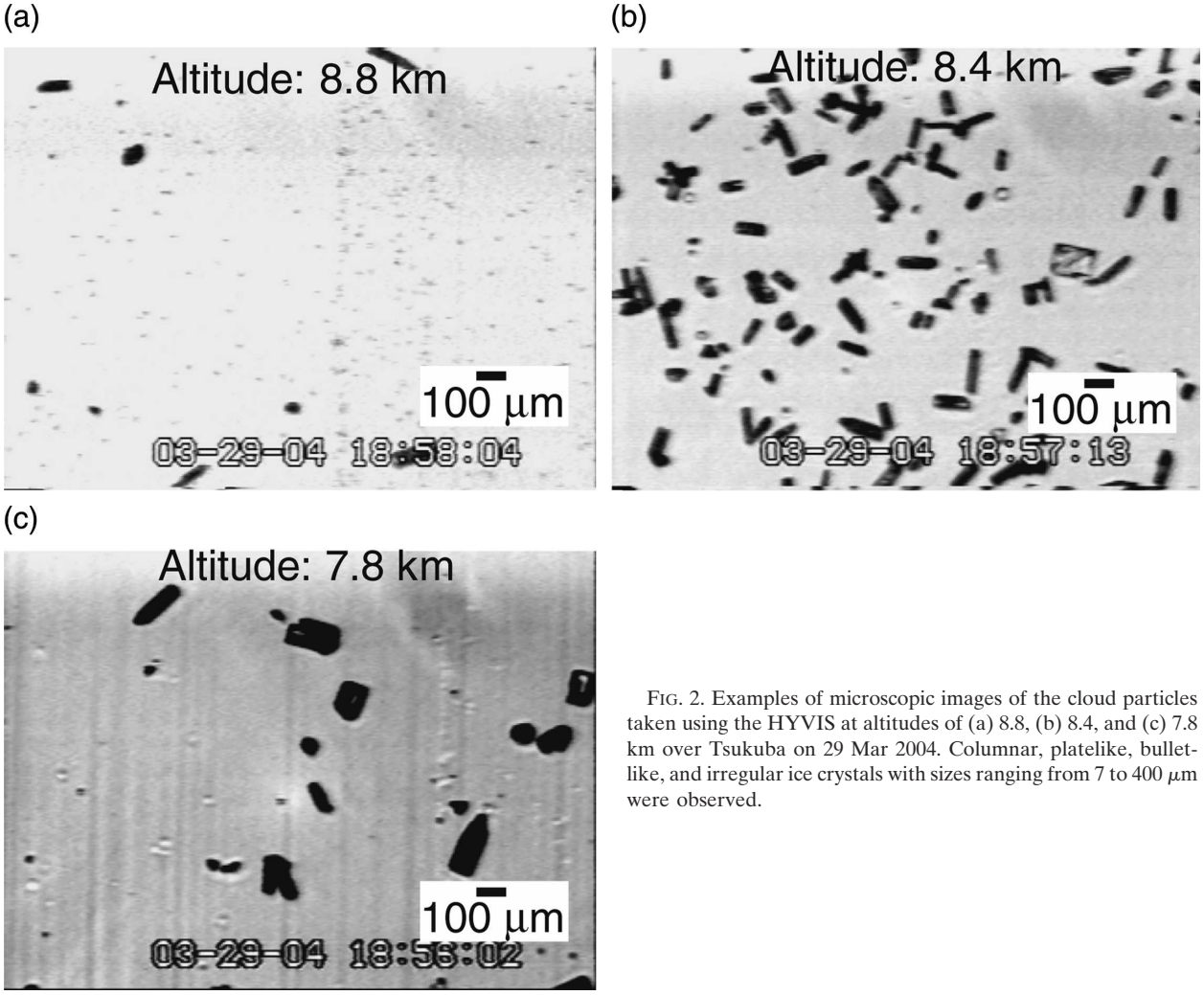

FIG. 2. Examples of microscopic images of the cloud particles taken using the HYVIS at altitudes of (a) 8.8, (b) 8.4, and (c) 7.8 km over Tsukuba on 29 Mar 2004. Columnar, platelike, bullet-like, and irregular ice crystals with sizes ranging from 7 to 400 μm were observed.

1802–0009 LST. Data with measurement uncertainties less than 10% for δ, 50% for S and RHi, and 100% for R and α are plotted in the figure. For the α and S values, the multiple scattering effect is not considered. The cross section of R (Fig. 1a) shows high values (>10) for an altitude range of 6–11 km. The values of δ were mostly 20%–35% for an altitude range of 5–11 km except for the middle region (Fig. 1b), indicating the predominance of randomly oriented large nonspherical particles in that region. These particles were probably ice crystals as revealed by the HYVIS measurement (Fig. 2). The values of S were mostly between 0.3 and 30 sr in that region. These values of δ and S are consistent with those reported by the previous measurements of cirrus clouds (Ansmann et al. 1992a,b; Sassen and Benson 2001; Sakai et al. 2003) and those calculated theoretically for the ice crystals (Takano and Liou 1989; Hess et al. 1998). It should be noted that these values showed low values ($\delta < 10\%$ and $S < 10$ sr) in the middle of the cloud (6.5–8 km in altitude, temperature ranged from −25.6° to −35°C). This was possibly due to the presence of horizontally oriented ice crystals that will be discussed in section 3c. The value of α in the cloud varied between 0.02 and 1.54 km^{-1} (Fig. 1d), and the optical thickness (τ) varied between 0.3 and 2.6. The relative humidity was saturated or slightly supersaturated with respect to ice (≥100%) in the lower part of the clouds (Fig. 1e), which supports the presence of the ice crystals.

b. HYVIS data

Figure 2 shows the examples of microscopic images of the cloud particles taken by the HYVIS at altitudes of 8.8, 8.4, and 7.8 km. The temperatures at the three altitudes were −39.3°, −36.7°, and −33.8°C, and RHi values at these altitudes were 106%, 96%, and 99% (measured using the SnowWhite hygrometer; see right panel of Fig. 4). Figure 2 shows that ice crystals were

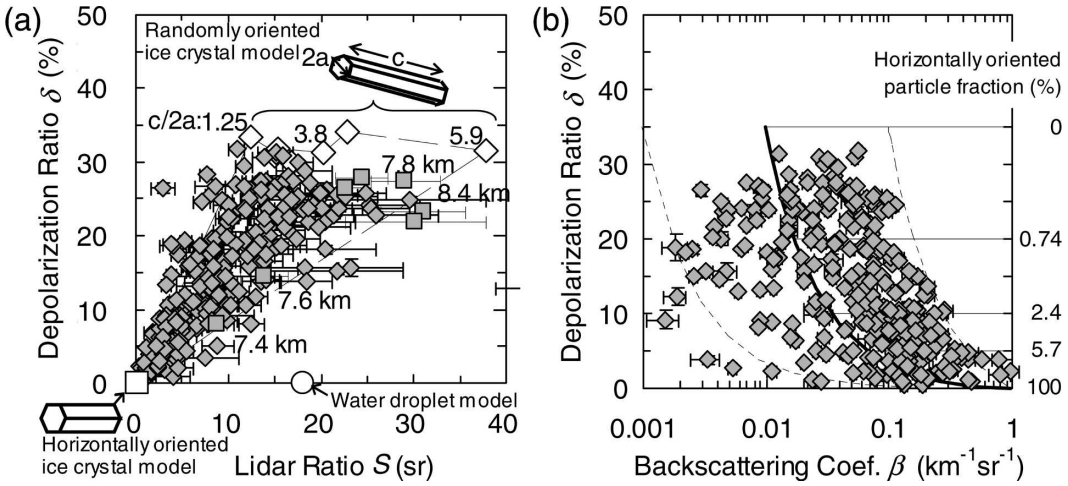

FIG. 3. Scatterplots of the particle depolarization ratio as a function of (a) the lidar ratio and (b) backscattering coefficient for the clouds. Solid diamonds represent values observed with the lidar in the clouds. Open symbols in (a) show the theoretical values for the randomly oriented hexagonal columns with aspect ratio between 1.25 and 5.9 (open diamonds), horizontally oriented ice crystal (open square), and water droplets (open circle). The numbers to the right of (b) are the number fraction of the horizontally oriented ice crystals that are estimated by assuming the backscattering cross-section ratio to be 100/1.

predominant at the three altitudes. The shape of the crystals was mostly columnar, bulletlike, platelike, and irregular. The crystal size (maximum dimension) was in the range of 7–400 μm. The mean particle size generally increased with decreasing height. The maximum size was 100–200 μm in the upper altitude region (8.25–11.5 km, Figs. 2a,b) and 250–400 μm in the lower region (6.0–8.25 km, Fig. 2c). A more detailed analysis of the cloud microphysical properties is given by Orikasa et al. (2006). The total particle number concentration ranged between 1 and 496 L^{-1} at altitudes between 5.0 and 11.5 km and was the highest at 8.25–8.5 km (Fig. 2b). It should be noted that few water droplets were detected with HYVIS. This result suggests that the ice crystals were predominant in the cloud and they produced the observed variations in δ and S, which is discussed in the following subsection.

c. *Relation between depolarization ratio and lidar ratio*

The lidar measurement showed that the values of δ and S varied as 0%–35% and 0.3–30 sr in the clouds (Figs. 1b,c). To study the observed variations of these values, we compare them with those calculated theoretically for the cloud particles. The result of the comparison is shown in Fig. 3a by the scatterplot of δ as a function of S. The lidar-observed values are shown for the cloud data taken between altitudes of 6.45–7.84 km for the period 1847–0009 LST (total 280 data points). The average uncertainties of the data are 0.2% for δ and 2 sr for S. The theoretical values are shown for the three cloud particles: 1) randomly oriented hexagonal ice columns whose prism-to-basal face axis ratio ($c/2a$) ranging from 1.25 to 5.9 calculated using the geometrical ray-tracing technique (Hess et al. 1998); 2) horizontally oriented ice crystals calculated using the geometrical ray-tracing technique (Liou and Lahore 1974), T-matrix method (Mishchenko et al. 1997), and the finite difference time domain (FDTD) method (Yang et al. 2003); and 3) water droplets (C1 model with an effective radius of 4 μm; Deirmendjian 1969) calculated using the Mie theory. In the case of the randomly oriented ice columns, the surface roughness was accounted by statistical deviations of ray paths during the ray tracing in the crystals; each time a ray hits a crystal surface, the normal to this surface is tilted with respect to its original direction by a certain angle and also rotated around it. The tilt angle is randomly distributed between 0°and 1°, whereas the azimuth angle is randomly distributed between 0° and 180°. The reasons for incorporating the surface roughness are that perfect hexagonal particles always show halos but are rarely observed in natural cirrus clouds, and that the asymmetry factor calculated for perfectly shaped crystals are higher than that observed (Hess et al. 1998). The calculated values for the ice columns ranged from $\delta = 33\%$ and $S = 12$ sr ($c/2a = 1.25$) to $\delta = 32\%$ and $S = 38$ sr ($c/2a = 5.9$). The theoretically calculated values of δ and S for the other randomly oriented ice crystal shapes (plate-, bullet rosette–, dendrite-, and aggregatelike) are similar

($\delta = 22\%$–36% and $S = 6$–19 sr) to these values except for highly distorted crystals, hollow columns, and small (a few micrometers) crystals that show high S values (>70 sr) (Hess et al. 1998; Yang and Liou 1998, 2000).

Figure 3a shows that the δ values decreased with decreasing values of S. Moreover, most of the lidar-observed values lie within the area enclosed by the triangle whose two vertices represent the theoretical values for the randomly oriented ice crystals with $c/2a = 1.25$ ($\delta = 33\%$ and $S = 12$ sr) and $c/2a = 5.9$ ($\delta = 32\%$ and $S = 38$ sr), and the third vertex of this triangle represents the values for the horizontally oriented ice crystals ($\delta = 0\%$ and $S < 1$ sr). This result suggests that the ice crystals were predominant in the cloud and that the proportion of the horizontally oriented crystals in the randomly oriented crystals varied therein. There are few measurement data showing values close to that for water droplets ($\delta = 0\%$ and $S = 18$ sr), suggesting that there were no regions wherein water droplets were predominant. This result is consistent with the results of the HYVIS measurement (e.g., Fig. 2) that showed that the water droplets were nearly absent for the detected size range (>7 μm). Although the small water droplets, which could not be detected by the HYVIS (<7 μm), could have been present where the temperatures were higher than the homogeneous freezing point of supercooled water (−40°C; below 8.7 km), the presence of these droplets was unlikely since they would have evaporated when the ice crystals coexisted because of the equilibrium water vapor pressure for supercooled water that is higher than ice.

To support the hypothesis of the presence of the horizontally oriented ice crystals, Fig. 3b shows the scatterplot of δ as a function of β for the cloud data. The average uncertainty of β is 10%. Figure 3b shows that δ decreased with increasing values of β. This is probably because the horizontally oriented crystals produce strong backscattering without depolarization by specular reflections (Liou and Lahore 1974; Platt et al. 1978; Mishchenko et al. 1997; Yang et al. 2003) and the fraction of them varies in the cloud.

Since β is the product of the backscattering cross section and the number concentration of the scattering particles, the number fraction of the horizontally oriented crystals in the randomly oriented crystals can be estimated by assuming the δ values and the ratio of the mean backscattering cross section for these particles as follows. If the backscattering by the ice crystals is predominant in the lidar-observed signal, the observed particle depolarization ratio can be expressed by

$$\delta = \frac{\delta_H \beta_H + \delta_R \beta_R}{\beta_H + \beta_R}, \tag{1}$$

where subscripts H and R denote the horizontally oriented and randomly oriented ice crystals, respectively, and the backscattering coefficients for these crystals are expressed by

$$\beta_X = N_X \frac{d\sigma_X}{d\Omega}, \tag{2}$$

where N_x is the crystal number concentration and $(d\sigma_X/d\Omega)$ is the mean backscattering cross section of the X-oriented crystals where X is H or R. Defining the number fraction of the horizontally oriented ice crystals by means of the expression, $f_H \equiv N_H/(N_H + N_R)$ and the ratio of the backscattering cross section of the horizontally oriented crystals to the randomly oriented crystals by $r \equiv (d\sigma_H/d\Omega)/(d\sigma_R/d\Omega)$, we can express Eq. (1) as follows:

$$\delta = \frac{\delta_H f_H r + \delta_R (1 - f_H)}{f_H r + (1 - f_H)}, \tag{3}$$

from which we obtain

$$f_H = \frac{\delta_R - \delta}{\delta(r - 1) - \delta_H r + \delta_R}. \tag{4}$$

The solid curve in Fig. 3b indicates a line for which f_H varies between 0 and 1 (from upper left to lower right). It is assumed that the δ values for the two oriented crystals are 0% and 35% based on the range of the measured values, r is 100 based on the theoretical calculation for the ice disk by Mishchenko et al. (1997), and the maximum value of β is 0.97 km^{-1} sr^{-1}. Under these assumptions of δ and r, the values of f_H are, for example, 0.74% at $\delta = 20\%$, 2.4% at $\delta = 10\%$, and 5.7% at $\delta = 5\%$. This estimation suggests that the variation in the small number fraction (a few particles per liter) of the horizontally oriented ice crystals produced the large variations in δ (and S) at the high values ($\delta > 10\%$), which has already been pointed out by Platt (1978) and Sassen and Benson (2001). However, we cannot verify this estimation using the HYVIS data because the HYVIS cannot measure the particle orientation without disturbing it during the sampling process. The observed data mostly lie between the lines of $r = 10$ and 1000 (dashed curves in Fig. 3b), thereby suggesting that the β ratios of the two oriented particles are between these values.

The vertical variations of δ and S (Figs. 1b,c) shows that these values were the lowest ($\delta < 10\%$ and $S < 10$ sr) in the middle of the clouds (6.5–8 km in altitude, see also Fig. 4), suggesting that the proportion of the horizontally oriented ice crystals were the largest in that region. The possible reason for the largest proportion of the horizontally oriented crystals in that region was

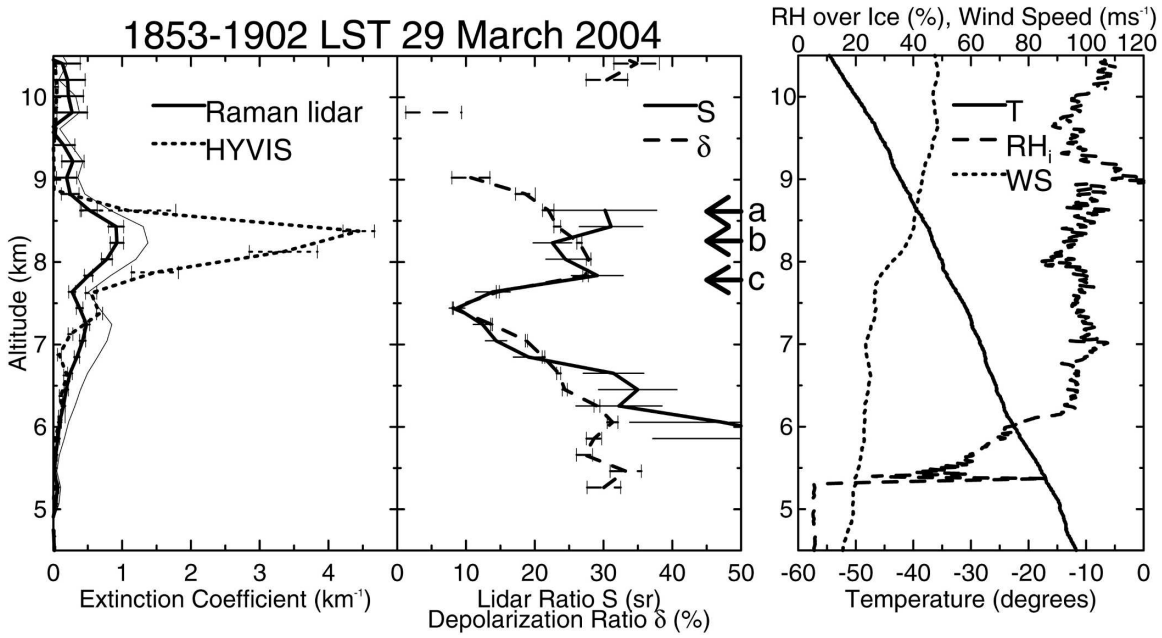

FIG. 4. Vertical profiles of (left) the particle extinction coefficients, (middle) lidar ratio and depolarization ratio. The solid lines in the left panel show the lidar-derived extinction with (thin solid) or without (thick solid) correction for the multiple scattering. The dotted line shows the HYVIS-derived extinction. The arrows in the middle panel show the altitudes where the micrographs (Fig. 2) were taken. (right) The temperature (solid line), relative humidity with respect to ice (dashed line), and horizontal wind speed (dotted line) obtained with the HYVIS-mounted balloon.

that the large-scale turbulence was weak in that region. The turbulence expected from the wind profile was not large (dotted line in the right panel of Fig. 4); this shows that the vertical shear of the horizontal wind was small (average of 1.69 m s^{-1} km^{-1} between 6.5 and 7.7 km). The corresponding average Richardson number is 105, which is much larger than the threshold (0.25) for the onset of the turbulence caused by the Kelvin–Helmholtz instability. Under the low shear conditions, large-scale turbulence was unlikely to occur; hence, the ice crystals aligned their longest axis parallel to the horizontal plane as falling in the air (Ono 1969). Accordingly, the proportion of the horizontally oriented crystals was the largest and hence δ and S were the lowest in this region.

The results obtained suggest that by measuring the S and δ values with the lidar, it is possible to distinguish the phase and orientation of the cloud particles: randomly oriented ice crystals ($\delta > 20\%$), horizontally oriented ice crystals ($\delta \sim 0$ and $S < 1$ sr), and water droplets ($\delta \sim 0$ and $S \sim 18$ sr). In addition, their individual fractions can be estimated. Such measurements might be useful for studying the radiative effect of clouds because their reflectance and absorptance critically depend on particle phase and orientation (Asano 1983; Takano and Liou 1989). However, this method should be verified by measuring mixed-phase clouds with the Raman lidar and HYVIS or other in situ instruments. Moreover, it is useful to measure the δ of ice clouds by tilting the lidar away from the vertical direction in order to verify the ice crystal orientation (Platt 1978; Thomas et al. 1990).

d. Comparison of particle extinction coefficient

To quantitatively compare the Raman lidar data and HYVIS data, Fig. 4 shows the vertical profiles of α obtained using the lidar and those calculated from the HYVIS data (left panel). In the cloud, the measurement uncertainty in α determined by the lidar is less than 20% (6.2–8.4 km); it increased to above 100% outside the cloud (below 5.5 km and above 9.4 km) due to the weak Raman-backscattered signal above the cloud and small extinctions. For the HYVIS data, the α values were calculated from the total particle cross-sectional area multiplied by 2, assuming the geometrical optics approximation because the particles were larger (7–400 μm) than the laser wavelength. The measurement uncertainty in the HYVIS data was estimated from the standard deviation of the total particle number concentrations in each height range. Figure 4 shows that the lidar-derived α (without multiple scattering correction; thick solid line) is 0.92 km^{-1} at the peak altitude of 8.2 km. This value is approximately 5 times lower than the HYVIS-derived value of 4.44 km^{-1}. The

lidar-derived optical thickness derived is 1.6 ± 0.1 between 5.0 and 10.5 km. This value is approximately 2 times lower than the HYVIS-derived value of 3.1. The possible reasons for the differences in α and τ between the two measurement data are as follows: 1) horizontal and temporal differences in the cloud properties between the measurements using the lidar and HYVIS, 2) underestimation of the lidar-derived values by neglecting the multiple scattering effect, and 3) overestimation of the HYVIS-derived values by altering the particle properties during the sampling process. Reason 1) is most likely because the horizontal distance between the two instruments was 16–19 km for the period when the HYVIS instrumented balloon was in the cloud for altitudes between 6.9–10.6 km (1853–1902 LST; Fig. 4). A large horizontal variation in the cloud properties can be expected from the temporal variations of R (Fig. 1a) and α (Fig. 1d). For example, the value of α is in the range of 0.08 to 1.45 km^{-1} at the peak altitude of 8.2 km and τ is in the range of 0.3 to 2.6. Although their maximum values are smaller than those determined by the HYVIS, the horizontal variations could be larger than the temporal variations over the lidar site. Reason 2) is possible because the lidar-derived α values could be underestimated with respect to the true values when the cloud particles scatter light strongly in the forward direction (e.g., Wandinger 1998; Reichardt et al. 2000; Sakai et al. 2003). This is because the forward-scattered light could be backscattered by nitrogen molecules, which reduces the apparent extinction of the Raman nitrogen signal. Using the model developed by Wandinger (1998), we have evaluated the influence of multiple scattering on the α values determined by our lidar (2-mrad receiver field of view). The result is shown by the thin solid line in Fig. 4. In the calculation, we assumed that the scattering phase function of the cloud particles was approximated by that of the randomly oriented hexagonal columns (Wandinger 1998) based on the HYVIS images that have shown that the columnar crystals were abundant (Fig. 2). The corrected α value is 1.37 km^{-1} at the peak altitude and τ is 2.7. These values are lower than those derived from the HYVIS data; therefore, the observed difference cannot be explained based on them alone. Reason 3) is possible because the HYVIS-derived values could be overestimated with regard to the true values by altering the cloud properties during the sampling processes. For example, the cross-sectional area of the cloud particles derived from the HYVIS images could overestimate the true value because the ice crystals (e.g., the platelike and columnar ones) could settle on the film of the instrument such that it maximizes its cross-sectional area. This can lead to the overestimation of the cross-sectional area if the ice crystals were randomly oriented in air. For example, the mean cross-sectional area of the randomly oriented hexagonal plates with an axis ratio of 1/5 is 56% of the maximum cross-sectional area, whereas that for the randomly oriented hexagonal column with an axis ratio of 5/1 is 77% of the maximum area. If we reduce the HYVIS-derived α by multiplying these factors, we obtain the values of 2.49 and 3.42 km^{-1}. These values are larger than the lidar-derived values. The other possible reason for the overestimation of the HYVIS-derived values is the uncertainty in the flow rate of air by the suction fan. Orikasa and Murakami (1997) have reported that the uncertainty in the flow speed of air is approximately 10% at atmospheric pressures higher than 300 hPa and increases to as large as 100% at 200 hPa. The pressure in the cloud (5.0–11.5 km in altitude) was between 542 and 211 hPa and it was approximately 340 hPa at the peak altitude. On the basis of these results, it is inferred that the error caused by the flow rate calculation is too small to explain the observed differences.

From these assessments, we conclude that horizontal inhomogeneity in the cloud properties is the most probable reason for the observed differences between the extinction values determined by the lidar and HYVIS. This result reveals the difficulty in the quantitative validation of the lidar measurement of cirrus optical properties using HYVIS data when the horizontal inhomogeneity is large. Nevertheless, simultaneous measurements performed using these instruments provide valuable information on cirrus properties such as phase, shape, size, number concentration, orientation, and optical properties. The measurement setup of the HYVIS is simple and can be launched every hour. Hence, successive launches of the HYVIS and continuous lidar measurements will be beneficial to the study of the evolution of cirrus clouds.

4. Conclusions

We measured the optical and microphysical properties of the upper clouds over Tsukuba on 29–30 March 2004 using the Raman lidar and HYVIS. The clouds were present at the altitude range of 5–11.5 km. The cloud particles were mostly ice crystals. The crystal shape was columnar, bulletlike, platelike, and irregular. The crystal size ranged from 7 to 400 μm. The number concentration varied between 1 and 496 L^{-1} and was the highest at an altitude range of 8.25–8.5 km. The particle depolarization ratio varied between 0%–35% and the lidar ratio varied between 0.3–30 sr in the clouds. The depolarization ratio generally decreased with decreasing values of the lidar ratio and increasing

values of backscattering coefficient. The comparison of these observed values with theoretical values suggests that the observed variations were due to the variation in the proportion of the horizontally oriented ice crystals in the clouds. The proportion of the horizontally oriented ice crystals was expected to be the largest at the middle of the clouds where the vertical shear of the horizontal wind was small. The particle extinction coefficient obtained with the lidar was approximately 5 times lower than that calculated from the HYVIS measurement data at the peak height. The cloud optical thickness obtained with the lidar was approximately 2 times lower than that obtained with the HYVIS. The most probable reason for the differences is the horizontal inhomogeneity of the particle properties between the measurement sites for the two instruments. The other possible reasons for the differences are the underestimation of the lidar-derived value by neglecting the multiple scattering effect and the overestimation of the HYVIS-derived value by altering the particle properties during the sampling process. Although the present study has revealed the difficulty in the quantitative validation of the lidar measurements of cirrus optical properties using HYVIS data, successive launching of HYVIS-mounted balloons and continuous lidar measurements will be beneficial to the study of the evolution of the microphysical and optical properties of cirrus clouds. These properties are required to facilitate a deeper understanding of their effects on climate.

Acknowledgments. This research was partly supported by a grant from the Ministry of Education, Culture, Sports, Science and Technology, Japan (Dynamics of the Sun-Earth-Life Interactive System, G-4, the 21st Century COE Program).

REFERENCES

Ackermann, J., 1998: The extinction-to-backscatter ratio of tropospheric aerosol: A numerical study. *J. Atmos. Oceanic Technol.,* **15,** 1043–1050.

Anderson, T. L., S. J. Masonis, D. S. Covert, and R. J. Charlson, 2000: In-situ measurement of the aerosol extinction-to-backscatter ratio at a polluted continental site. *J. Geophys. Res.,* **105,** 26 907–26 915.

Ansmann, A., 2002: Molecular-backscatter lidar profiling of the volume-scattering coefficient in cirrus. *Cirrus,* D. Lynch, K. Sassen, D. O'C. Starr, and G. L. Stephens, Eds., Oxford University Press, 197–210.

——, U. Wandinger, M. Riebesell, C. Weitkamp, and W. Michaelis, 1992a: Independent measurement of extinction and backscatter profiles in cirrus cloud by using a combined elastic-backscatter lidar. *Appl. Opt.,* **31,** 7113–7131.

——, ——, ——, ——, E. Voss, W. Lahmann, and W. Michaelis, 1992b: Combined Raman elastic-backscatter LIDAR for vertical profiling of moisture, aerosol extinction, backscatter, and LIDAR ratio. *Appl. Phys.,* **B55,** 18–28.

Asano, S., 1983: Transfer of solar radiation in optically anisotropic ice clouds. *J. Meteor. Soc. Japan,* **61,** 402–413.

Deirmendjian, D., 1969: *Electromagnetic Scattering on Spherical Polydispersions*. Elsevier, 78 pp.

Ferrare, R. A., D. D. Turner, L. H. Brasseur, W. F. Fertz, O. Dubovik, and T. Tooman, 2001: Raman lidar measurements of the aerosol extinction-to-backscatter ratio over the Southern Great Plains. *J. Geophys. Res.,* **106,** 20 333–20 347.

Hess, M., R. B. A. Koelemeijer, and P. Stammes, 1998: Scattering matrices of imperfect hexagonal ice crystals. *J. Quant. Spectrosc. Radiat. Transfer,* **60,** 301–308.

Hogan, R. J., P. N. Francis, H. Flentje, A. J. Illingworth, M. Quante, and J. Pelon, 2003: Characteristics of mixed-phase clouds. Part I: Lidar, radar and aircraft observations from CLARE'98. *Quart. J. Roy. Meteor. Soc.,* **129,** 2089–2116.

Kusunoki, K., M. Murakami, M. Hashimoto, N. Orikasa, Y. Yamada, H. Mizuno, K. Hamazu, and H. Watanabe, 2004: The characteristics and evolution of orographic snow clouds under weak cold advection. *Mon. Wea. Rev.,* **132,** 174–191.

Liou, K. N., 1986: Influence of cirrus clouds on weather and climate processes: A global perspective. *Mon. Wea. Rev.,* **114,** 1167–1198.

——, and H. Lahore, 1974: Laser sensing of cloud composition: A backscattered depolarization technique. *J. Appl. Meteor.,* **13,** 257–263.

Mishchenko, M. I., and K. Sassen, 1998: Depolarization of lidar returns by small ice crystals: An application to contrails. *Geophys. Res. Lett.,* **103,** 309–312.

——, D. J. Wielaard, and B. E. Carlson, 1997: T-matrix computations of zenith-enhanced lidar backscatter from horizontally oriented ice plates. *Geophys. Res. Lett.,* **24,** 771–774.

Mizuno, H., T. Matsuo, M. Murakami, and Y. Yamada, 1994: Microstructure of cirrus clouds observed by HYVIS. *Atmos. Res.,* **32,** 115–124.

Murakami, M., and T. Matsuo, 1990: Development of the hydrometeor videosonde. *J. Atmos. Oceanic Technol.,* **7,** 613–620.

Murakami, M., Y. Yamada, T. Matsuo, and H. Mizuno, 1992: Microphysical structures of warm-frontal clouds—The 20 June 1987 case study. *J. Meteor. Soc. Japan,* **70,** 877–895.

Ono, A., 1969: The shape and riming properties of ice crystals in natural clouds. *J. Atmos. Sci.,* **26,** 138–147.

Orikasa, N., and M. Murakami, 1997: A new version of hydrometeor videosonde for cirrus cloud observations. *J. Meteor. Soc. Japan,* **75,** 1033–1039.

——, and ——, 2006: Characteristics of cirrus crystal shapes from hydrometeor videosonde data. Preprints, *12th Conf. on Cloud Physics,* Madison, WI, Amer. Meteor. Soc., CD-ROM, P1.53.

Platt, C. M. R., 1978: Lidar backscatter from horizontal ice crystals plates. *J. Appl. Meteor.,* **17,** 482–488.

——, N. L. Abshire, and G. T. McNice, 1978: Some microphysical properties of an ice cloud from lidar observation of horizontally oriented crystals. *J. Appl. Meteor.,* **17,** 1220–1224.

Reichardt, J., M. Hess, and A. Macke, 2000: Lidar inelastic multiple-scattering parameters of cirrus particle ensembles determined with geometrical-optics crystal phase functions. *Appl. Opt.,* **39,** 1895–1910.

——, S. Reichardt, A. Behrendt, and T. J. McGee, 2002: Correlations among the optical properties of cirrus-cloud particles: Implications for spaceborne remote sensing. *Geophys. Res. Lett.,* **29,** 1668, doi:10.1029/2002GL014836.

Sakai, T., T. Nagai, M. Nakazato, and T. Matsumura, 2003: Ice clouds and Asian dust studied with lidar measurements of particle extinction-to-backscatter ratio, particle depolarization, and water vapor mixing ratio over Tsukuba. *Appl. Opt.,* **42,** 7103–7116.

Sassen, K., and S. Benson, 2001: A midlatitude cirrus cloud climatology from the Facility for Atmospheric Remote Sensing. Part II: Microphysical properties derived from lidar depolarization. *J. Atmos. Sci.,* **58,** 2103–2112.

——, W. P. Arnott, D. O'C. Starr, G. G. Mace, Z. Wang, and M. R. Poellot, 2003: Midlatitude cirrus clouds derived from hurricane Nora: A case study with implications for ice crystals nucleation and shape. *J. Atmos. Sci.,* **60,** 873–891.

Stephens, G. L., 2002: Cirrus, climate, and global change. *Cirrus,* D. Lynch, K. Sassen, D. O'C. Starr, and G. L. Stephens, Eds., Oxford University Press, 433–448.

Takano, Y., and K. N. Liou, 1989: Solar radiative transfer in cirrus clouds. Part II: Theory and computation of multiple scattering in an anisotropic medium. *J. Atmos. Sci.,* **46,** 20–36.

Thomas, L., J. C. Cartwright, and D. P. Wareing, 1990: Lidar observations of the horizontal orientation of ice crystals in cirrus clouds. *Tellus,* **42B,** 211–216.

Wandinger, U., 1998: Multiple-scattering influence on extinction- and backscatter-coefficient measurements with Raman and High-Spectral-Resolution Lidars. *Appl. Opt.,* **37,** 417–427.

Whiteman, D. N., 2003: Raman lidar. *Encyclopedia of Atmospheric Sciences,* J. R. Holton, Ed., Academic Press, 1202–1212.

Whiteway, J., and Coauthors, 2004: Anatomy of cirrus clouds: Results from the Emerald airborne campaigns. *Geophys. Res. Lett.,* **31,** L24102, doi:10.1029/2004GL021201.

Yang, P., and K. N. Liou, 1998: Single-scattering properties of complex ice crystals in terrestrial atmosphere. *Contrib. Atmos. Phys.,* **71,** 223–248.

——, and ——, 2000: Finite difference time domain method for light scattering by nonspherical and nonhomogeneous particles. *Light Scattering by Nonspherical Particles: Theory, Measurements and Applications,* M. I. Mishchenko, J. W. Hovenier, and L. D. Travis, Eds., Academic Press, 173–221.

——, Y. X. Hu, D. M. Winker, J. Zhao, C. A. Hosteller, B. A. Baum, M. I. Mishchenko, and J. Reichardt, 2003: Enhanced lidar backscattering by horizontally oriented ice plates. *J. Quant. Spectrosc. Radiat. Transfer,* **79-80,** 1139–1157.